GA–A27938

ELECTRON TEMPERATURE CRITICAL GRADIENT AND TRANSPORT STIFFNESS

by
S.P. SMITH, C.C. PETTY, A.E. WHITE, C. HOLLAND, R.V. BRAVENEC, M.E. AUSTIN, L. ZENG, and O. MENEGHINI

SEPTEMBER 2014

GENERAL ATOMICS

DISCLAIMER

GA–A27938

ELECTRON TEMPERATURE CRITICAL GRADIENT AND TRANSPORT STIFFNESS

by
S.P. SMITH, C.C. PETTY, A.E. WHITE,* C. HOLLAND,† R.V. BRAVENEC,‡ M.E. AUSTIN,‡
L. ZENG,¶ and O. MENEGHINI§

This is a preprint of a paper to be presented at the Twenty-Fifth IAEA Fusion Energy Conf., October 13-18, 2014 in Saint Petersburg, Russia and published in the *Proceedings.*

*Massachusetts Institute of Technology, Cambridge, Massachusetts.
†University of California San Diego, La Jolla, California.
‡University of Texas at Austin, Austin, Texas.
¶University of California Los Angeles, Los Angeles, California.
§Oak Ridge Associated Universities, Oak Ridge, Tennessee.

Work supported by
the U.S. Department of Energy
under DE-FC02-04ER54698, DE-FC02-99ER54512,
DE-FG02-06ER54871, DE-FG03-97ER54415, and DE-FG02-08ER54984

GENERAL ATOMICS PROJECT 30200
SEPTEMBER 2014

Electron Temperature Critical Gradient and Transport Stiffness

S.P. Smith[1], C.C. Petty[1], A.E. White[2], C. Holland[3], R. Bravenec[4], M.E. Austin[5], L. Zeng[6] and O. Meneghini[7]

[1]General Atomics, PO Box 85608, San Diego, CA 92186-5608, USA
[2]Massachussets Institute of Technology, 77 Massachusetts Ave, Cambridge, MA 02139, USA
[3]University of California San Diego, 9500 Gilman Dr., La Jolla, CA 92093-0417, USA
[4]Fourth State Research, 503 Lockhart Dr., Austin, TX 78704, USA
[5]University of Texas at Austin, 2100 San Jacinto Blvd, Austin, TX 78712-1047, USA
[6]University of California Los Angeles, PO Box 957099, Los Angeles, CA 90095, USA
[7]Oak Ridge Associated Universities, Oak Ridge, TN, USA

Corresponding Author: smithsp@fusion.gat.com

Abstract:
In a continuing effort to validate turbulent transport models, the electron energy flux has been probed as a function of electron temperature gradient on the DIII-D tokamak. In the scan of gradient, a critical electron temperature gradient has been found in the electron heat fluxes and stiffness at various radii in L-mode plasmas. The TGLF reduced turbulent transport model [G.M. Staebler, J.E. Kinsey, and R.E. Waltz, Phys. Plasmas 14, 055909 (2007)] and full gyrokinetic GYRO model [J. Candy and R.E. Waltz, J. Comput. Phys. 186, 545 (2003)] recover the general trend of increasing electron energy flux with increasing electron temperature gradient scale length, but they do not predict the absolute level of transport at all radii and gradients. Comparing the experimental observations of incremental (heat pulse) diffusivity and stiffness to the models' reveals that TGLF reproduces the trends in increasing diffusivity and stiffness with increasing electron temperature gradient scale length. A rotation reversal is observed for changing the value of the safety factor at the 95% flux surface from $q_{95} = 8.6$ to 4.3.

1 Introduction

As the cost of constructing new tokamaks balloons, and as future devices will have less area for diagnostics, it is vital to have a set of validated codes for prediction and interpretation of results. One method of validating the codes is to perform a systematic parametric scan in an experiment, to be able to compare cleanly to simulation. Using localized electron cyclotron heating (ECH) or minority ion cyclotron heating, the local electron or ion temperature gradient had previously been varied under a variety of conditions to probe the underlying physics, and provide comparisons against simulations. [1–9] In addition

to probing the steady state energy flow, the heating systems have been pulsed in such a way to allow for the probing of the heat pulse diffusivity and therefore stiffness of the plasma profiles. [3–6, 9, 10] A previously identified regime where the prediction of plasma transport by some gyrokinetic codes is incorrect is the low-confinement regime (L-mode) edge region [11–14], dubbed the "L-mode edge shortfall". Part of the inspiration for the experiments reported in the present work at the outer radii was to try to understand if the shortfall at outer radii is due to a failure of the gyrokinetic codes to predict the critical gradients and stiffness that the plasma exhibits in this region.

In this paper, we report on electron temperature gradient scale length scans in the DIII-D tokamak [15] at $\rho = 0.4$ and 0.7 with similar values of q_{95} and one scan at $\rho = 0.7$ for a lower value of q_{95}. We also report on the corresponding modeled fluxes and stiffness from the TGLF code [16] and some modeled linear growth rates and fluxes from the GYRO code. [17]

The experimental and modeling methods are laid out in section 2. The experimental inferences and gyrokinetic predictions of energy flux, heat pulse diffusivity, and stiffness are compared in section 3. Finally, the summary is presented in section 4.

2 Methods

2.1 Experimental

In the DIII-D tokamak, we have employed the electron cyclotron heating systems (gyrotrons) to locally heat the electrons. By aiming all six of the gyrotrons at the same initial location, then moving the gyrotrons one by one to a second location in subsequent discharges, a scan in electron temperature T_e and temperature gradient ∇T_e can be realized midway between the two aiming locations. Using this method, we have scanned ∇T_e at relatively constant T_e by depositing ECH power on either side of $\rho = 0.4$ (see FIG. 1a), $\rho = 0.6$ [6, 8, 9], and $\rho = 0.7$ (see FIG. 1b,c), where ρ is the normalized toroidal flux. The toroidal field across these scans is 1.98–2.02 T. The scans at $\rho = 0.4, 0.6$ had 0.8 MA plasma current; the scans at $\rho = 0.7$ had currents of 0.6 and 1.2 MA for q_{95} values of 8.6 and 4.3, respectively.

In these discharges, there is no beam heating, such that there is no external beam torque on the plasma, nor any central particle fueling. It is interesting to observe that the plasma rotation can depend on q_{95} or even just the ECH deposition location. In FIG. 2 the toroidal rotation profile fits are shown for the $\rho = 0.4$ case (a), the $\rho = 0.7$ $q_{95} = 8.6$ case (b), and the $\rho = 0.7$ $q_{95} = 4.3$ case (c). The color coding for the lines is the same as the corresponding temperature profiles in FIG. 1. In FIG. 2a and c, there is a clear trend of decreasing inner rotation with decreasing inner ECH deposition (red to blue). Comparing the cases in FIG. 2b and c, there is a rotation reversal for the change in plasma current from 1.2 MA in b to 0.6 MA in c. However, this is not the only parameter that is changing. The profiles of the electron density n_e and ion temperature T_i are shown in FIG. 3, where it is seen that the $q_{95} = 8.6$ (dashed) and $q_{95} = 4.3$ (dotted) n_e and T_i are different and could also contribute to the rotation reversal.

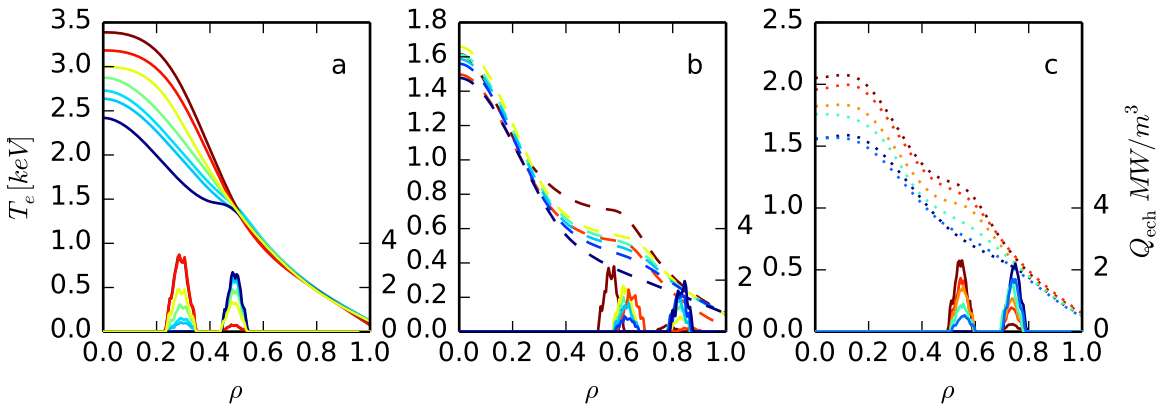

FIG. 1: Spline fits to electron temperature T_e measured by the electron cyclotron emission diagnostic (left scales) and calculated volumetric electron cyclotron heating (right scales) vs normalized toroidal flux ρ for a) the $\rho = 0.4$ case, b) the $\rho = 0.7$, $q_{95} = 8.6$ case, and c) the $\rho = 0.7$, $q_{95} = 4.3$ case.

One of the gyrotrons was always left in the outer location and modulated at 28Hz for all cases. This modulation allows the experimental heat pulse diffusivity to be determined. [6]

2.2 Simulation

The experimental profiles were used as inputs to the gyrofluid code TGLF [16] and to the gyrokinetic code GYRO [17] to obtain predictions of the microstability linear growth rates or turbulence driven plasma transport fluxes. The TGLF results presented here include the recent recalibration of the model. [18]

The linear growth rates and frequencies for the lowest and highest gradients (left and right panels) and a moderate gradient (middle panel) for the $\rho = 0.7$ $q_{95} = 8.6$ cases are in FIG. 4. Note the change in frequency of the dominant mode as the gradient is increased from the lowest gradient; this would indicate a change from an ITG type mode to a more TEM type mode. That the growth rate continues to increase with increasing ∇T_e indicates that the mode is a ∇T_e driven TEM.

3 Comparisons

Part of the motivation for performing these experiments was to be able to compare the experimental results with simulations to validate the models in the simulations. Here we provide comparisons of the fluxes, heat pulse diffusivities, and stiffnesses.

3.1 Power balance fluxes

The experimental power balance fluxes are calculated with the ONETWO code [19, 20], which accesses the ray tracing code TORAY-GA [21] to calculate the ECH power deposition. In FIG. 5, the electron Q_e (a,d,g), ion Q_i (b,e,h), and summed $Q_e + Q_i$ (c,f,i) energy

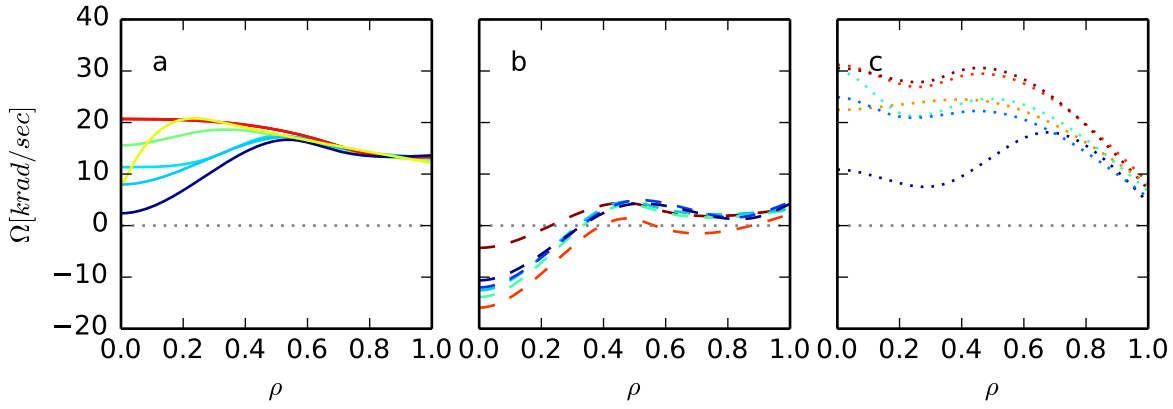

FIG. 2: Spline fits to Carbon VI toroidal rotation measurements Ω vs ρ for the a) $\rho = 0.4$ case b) $\rho = 0.7$ $q_{95} = 8.6$ case and c) $\rho = 0.7$ $q_{95} = 4.3$ case. Line coloring is the same as that for the T_e profiles of FIG. 1.

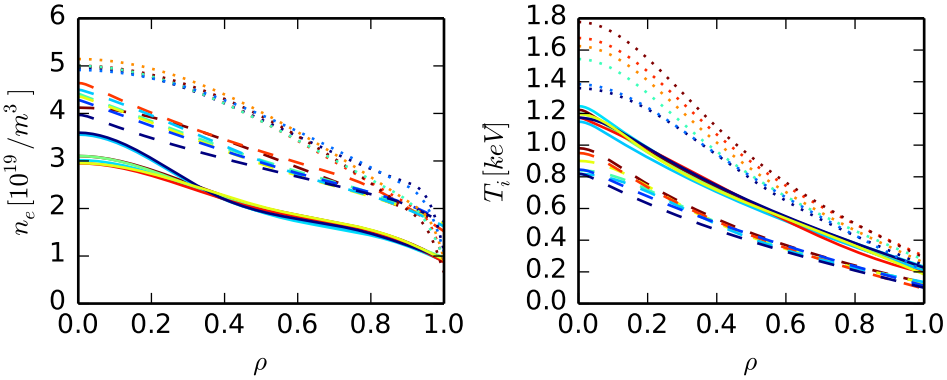

FIG. 3: Electron density n_e (left) and ion temperature T_i (right) vs ρ for the (solid) $\rho = 0.4$ case; (dashed) $\rho = 0.7$, $q_{95} = 8.6$ case; and (dotted) $\rho = 0.7$, $q_{95} = 4.3$ case.

fluxes are shown versus the normalized ∇T_e scale length a/L_{T_e} for the $\rho = 0.4$ case (a,b,c), the $\rho = 0.7$ $q_{95} = 8.6$ case (d,e,f), and the $\rho = 0.7$ $q_{95} = 4.3$ case (g,h,i). The experimentally calculated fluxes are shown as ○. The sum of the TGLF fluxes (for turbulence) and NEO fluxes (for neoclassical, but usually negligible for electrons) are given as □. The sum of the GYRO fluxes (for turbulence) and NEO fluxes are given as ◊, for the smallest, medium, and largest gradients of the $\rho = 0.7$ $q_{95} = 8.6$ case. Finally, there is a numerical scan of a/L_{T_e} for TGLF shown as the dashed curve, whose other parameters come from the experimental parameters of the point with the second highest gradient. Consistent with the motivation for the experiments at $\rho = 0.7$, TGLF and GYRO significantly underpredict the ion fluxes for the $\rho = 0.7$ cases, in spite of predicting the electron fluxes fairly well. At $\rho = 0.4$ TGLF actually overpredicts both the ion and electron fluxes.

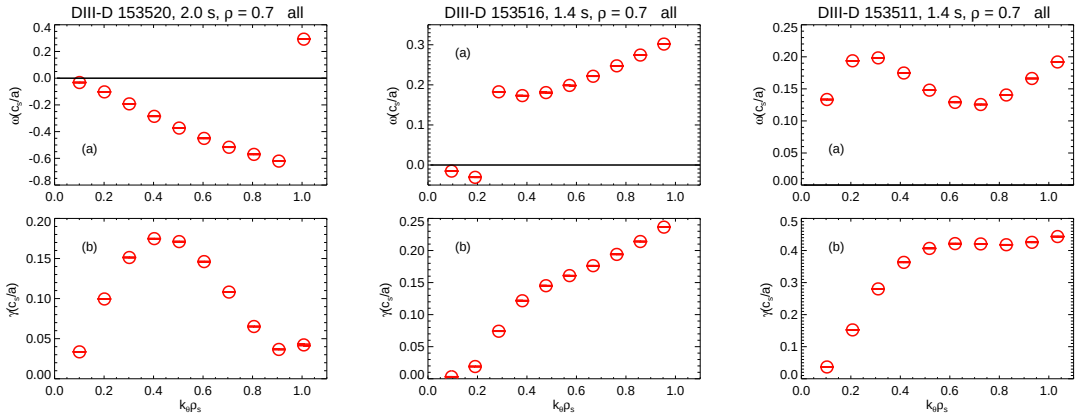

FIG. 4: GYRO predicted linear frequencies (top) and growth rates (bottom) for the smallest (left), moderate (middle) and highest (right) T_e gradients for the $\rho = 0.7$ $q_{95} = 8.6$ case. Positive frequency indicates a mode in the electron diamagnetic direction.

3.2 Diffusivities and Stiffness

Let us decompose the power balance energy flux into two parts

$$Q_e^{\rm PB} = -n_e D_e^{\rm PB} \nabla T_e + F, \tag{1}$$

where $\partial F/\partial \nabla T_e = 0$. Let us define the heat pulse diffusivity as

$$D_e^{\rm HP} = -\frac{1}{n_e}\frac{\partial Q_e^{\rm PB}}{\partial \nabla T_e} = \frac{\partial}{\partial \nabla T_e}(D_e^{\rm PB}\nabla T_e). \tag{2}$$

From the final form of (2), the power balance diffusivity $D_e^{\rm PB}$ can be solved as

$$D_e^{\rm PB} = \frac{1}{\nabla T_e}\int_0^{\nabla T_e} D_e^{\rm HP}{\rm d}(\nabla T_e). \tag{3}$$

The stiffness is then defined as

$$S = D_e^{\rm HP}/D_e^{\rm PB}. \tag{4}$$

In the experiment, the heat pulse diffusivity $D_e^{\rm HP}$ can be extracted from Fourier analysis of the ECE T_e measurements, which are modulated by the single modulated gyrotron. [6] For the TGLF code, $D_e^{\rm HP}$ is obtained by modifying the ∇T_e input to the code by 10% to obtain an incremental $Q_e^{\rm PB,inc}$, then taking the ratio $(Q_e^{\rm PB,inc} - Q_e^{\rm PB})/(1.1\nabla T_e - \nabla T_e)/n_e$. In both the experimental and TGLF cases $D_e^{\rm PB}$ is calculated from $D_e^{\rm HP}$ according to (3), where the value of $D_e^{\rm HP}\big|_{\nabla T_e=0}$ is defined as $D_e^{\rm HP}\big|_{\nabla T_e=\min(\nabla T_e)}$.

In FIG. 6 are shown the experimental ○ and TGLF □ $D_e^{\rm HP}$ (panels a and d), $D_e^{\rm PB}$ (panels b and e), and stiffness (panels c and f) for the $\rho = 0.7$ $q_{95} = 8.6$ case (panels a, b, and c) and $\rho = 0.7$ $q_{95} = 4.3$ case (panels d, e, and f). The dashed curve is obtained from the strict ∇T_e scan of TGLF, shown as the dashed curve in FIG. 5. The TGLF results agree with the broad experimental trends of increasing $D_e^{\rm HP}$ and $D_e^{\rm PB}$ with

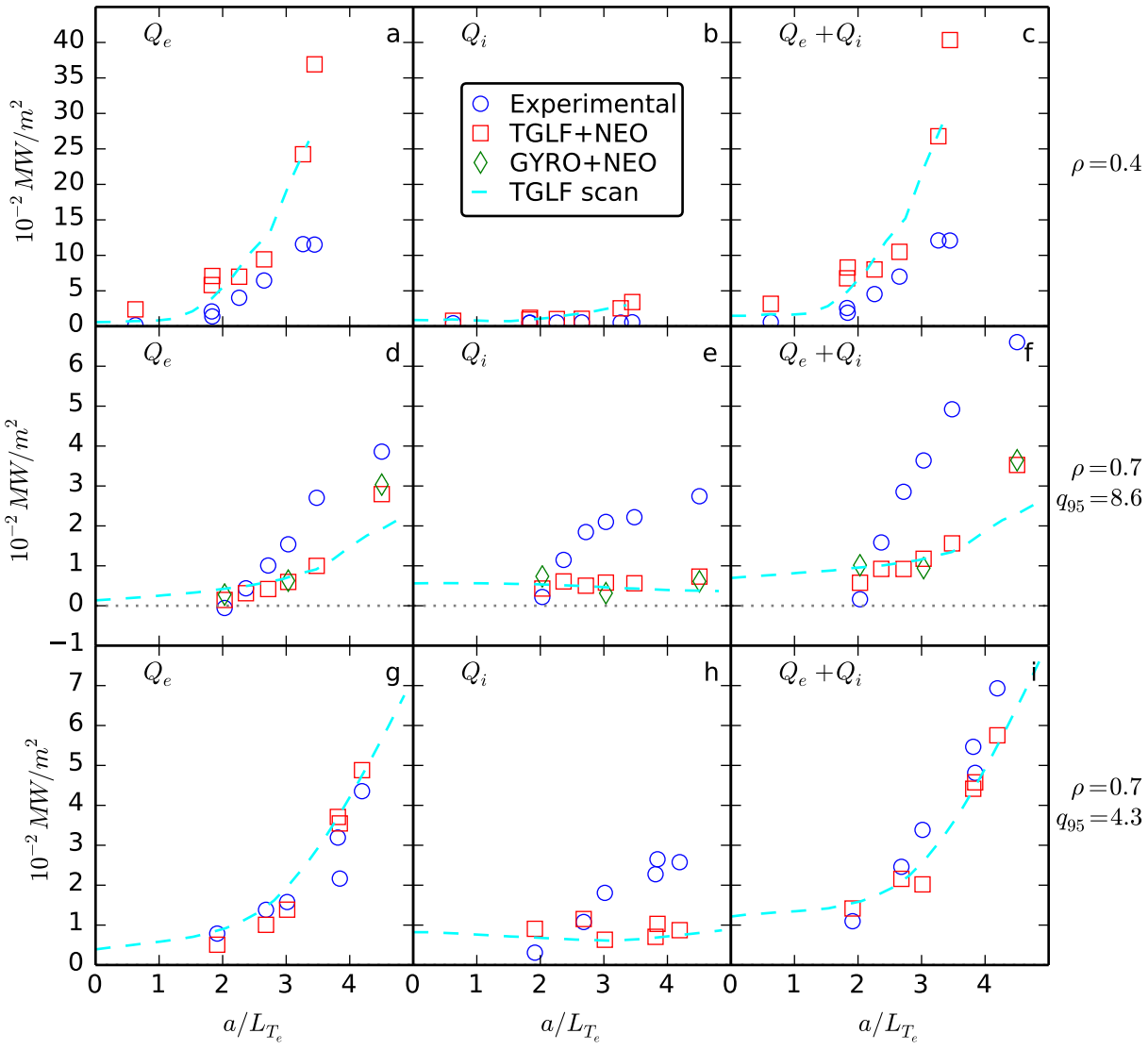

FIG. 5: The electron (a,d,g), ion (b,e,h) and total (c,f,i) energy fluxes vs the electron temperature gradient scale length for the $\rho = 0.4$ case (a,b,c), the $\rho = 0.7$ $q_{95} = 8.6$ case (d,e,f), and the $\rho = 0.7$ $q_{95} = 4.3$ case (g,h,i). The ○ are experimental points; the □ are predictions from TGLF; the ◊ are predictions from GYRO; the dashed curves are TGLF predictions from a scan in a/L_{T_e} based on the experimental conditions corresponding to the second largest value of a/L_{T_e} for each case.

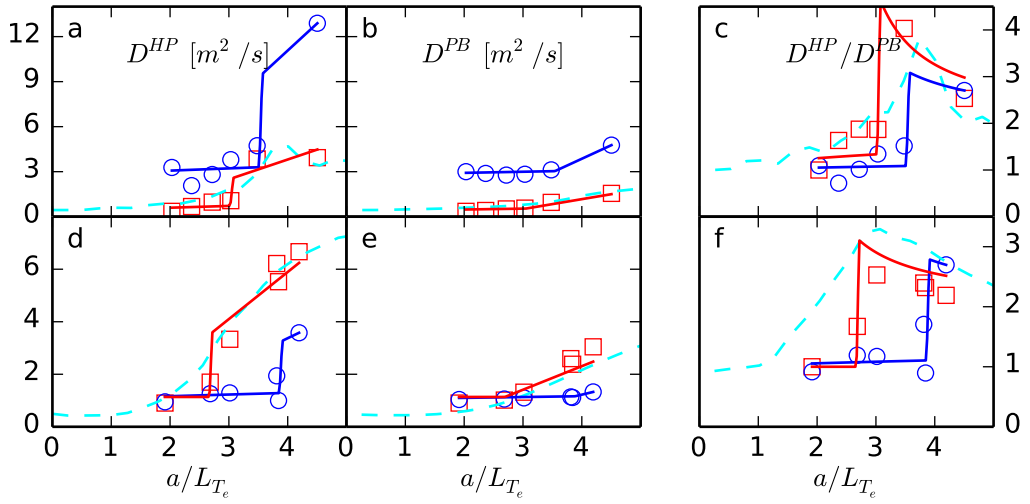

FIG. 6: Experimental ○ and TGLF □ heat pulse diffusivity (panels a and d), power balance diffusivity (panels b and e), and stiffness (panels c and f) vs a/L_{T_e} for the $\rho = 0.7$ $q_{95} = 8.6$ case (panels a-c) and $\rho = 0.7$ $q_{95} = 4.3$ case (panels d-f).

increasing a/L_{T_e}. Also shown as solid curves are a fit to $D_e^{\rm PB}$ and resulting $D_e^{\rm HP}$ and stiffness for each case for a model having two linear segments joined at $a/L_{T_e}^{crit}$. The fits yield values of $a/L_{T_e}^{crit}$ of 3.5 and 3.0 for experiment and TGLF at $q_{95} = 8.6$, and 3.9 and 2.7 for experiment and TGLF at $q_{95} = 4.3$. These values of $a/L_{T_e}^{crit}$ are consistent with the stiffness transitioning from below 2 to above 2 at these values of a/L_{T_e}. The increase in stiffness at the critical gradient is consistent with the change in character of the linear growth rates from an ion mode to an electron mode.

4 Conclusion

In the DIII-D tokamak, we have performed scans in a/L_{T_e} at various radii, with a sufficient range to see that a critical gradient has been exceeded to dominantly excite TEM more than ITG type turbulence based on the gyrokinetic linear growth rates. The change in nature of the dominant instability can be seen by its effect on the momentum transport (rotation profile) and by the increased dependence of the energy fluxes on a/L_{T_e} leading to an increase in stiffness of the electron heat flux with regard to a/L_{T_e}. The TGLF and GYRO models predict electron energy fluxes similar to that inferred from experiment, but the ion energy fluxes are underpredicted for the $\rho = 0.7$ cases, regardless of the value of q_{95} in the experiment. Focussing on the electron transport, the trends of increasing heat pulse diffusivity and stiffness from TGLF compares well to the experimental observations. A critical gradient is seen in both experiment and TGLF that depends on the q_{95} condition. The TGLF stiffness and critical gradient of the $q_{95} = 8.6$ case is closer to experiment than the $q_{95} = 4.3$ case, and yet the electron energy fluxes match better for the $q_{95} = 4.3$ case. The shortfall in prediction of ion energy fluxes is equally bad in the two $\rho = 0.7$ cases,

regardless of q_{95} or agreement with the electron temperature critical gradient or stiffness, indicating that a failure to get these features correct is not the cause of the shortfall. A better experiment may be a variation of ion temperature gradient in the outer radii to probe the ion temperature critical gradient and stiffness, since the shortfall is mostly in the ion channel.

Acknowledgements This material is based upon work supported by the U.S. Department of Energy, Office of Science, Office of Fusion Energy Sciences, using the DIII-D National Fusion Facility, a DOE Office of Science user facility, under Awards DE-FC02-04ER54698,DE-FC02-99ER54512, DE-FG02-08ER54871, DE-FG03-97ER54415, and DE-FG02-08ER54984.

References

[1] J.C DeBoo, et al. *Nuclear Fusion*, **45**(6), 494–501, Jun 2005.

[2] A. G. Peeters, et al. *Physics of Plasmas*, **12**(2), 022505, (2005).

[3] F. Ryter, et al. *Physical Review Letters*, **95**(8), 085001, Aug 2005.

[4] P. Mantica, et al. *Physical Review Letters*, **102**(17), 175002, Apr 2009.

[5] P. Mantica, et al. *Physical Review Letters*, **107**(13), 135004, Sep 2011.

[6] J. C. DeBoo, et al. *Physics of Plasmas*, **19**(8), 082518, Aug 2012.

[7] B Baiocchi, et al. *Plasma Physics and Controlled Fusion*, **55**(2), 025010, Feb 2013. Rotation gradient has more impact on stiffness than rotation magnitude.

[8] J. Hillesheim, et al. *Physical Review Letters*, **110**(4), 045003, Jan 2013.

[9] C. Holland, et al. *Nuclear Fusion*, **53**(8), 083027, Aug 2013.

[10] F. Ryter, et al. *Nuclear Fusion*, **51**(11), 113016, Nov 2011.

[11] C. Holland, et al. *Physics of Plasmas*, **16**(5), 052301, May 2009.

[12] T.L. Rhodes, et al. *Nuclear Fusion*, **51**(6), 063022, Jun 2011.

[13] N. T. Howard, et al. *Physics of Plasmas*, **21**(3), 032308, Mar 2014.

[14] D. Told, et al. *Physics of Plasmas*, **20**(12), 122312, Dec 2013.

[15] J.L. Luxon. *Nuclear Fusion*, **42**(5), 614–633, May 2002.

[16] G. M. Staebler, et al. *Physics of Plasmas*, **14**(5), 055909, May 2007.

[17] J. Candy and R.E. Waltz. *Journal of Computational Physics*, **186**(2), 545–581, Apr 2003.

[18] G. M. Staebler, *Private Communication*, 20 Aug 2014.

[19] W W Pfeiffer, et al. ONETWO: A computer code for modeling plasma transport in tokamaks. Technical Report GA-A16178, General Atomics, December 1980.

[20] H St. John, et al.Transport simulation of negative magnetic shear discharges. In *Plasma Physics and Controlled Nuclear Fusion Research 1994*, volume 3, pages 603–614. International Atomic Energy Agency, (1994).

[21] K. Matsuda. *IEEE Transactions on Plasma Science*, **17**(1), 6–11, (1989).